Periodico di Mineralogia (2011), 80, 1 (Special Issue), 27-38 DOI: 10.2451/2011PM0003

PERIODICO di MINERALOGIA
established in 1930

An International Journal of
MINERALOGY, CRYSTALLOGRAPHY, GEOCHEMISTRY, ORE DEPOSITS, PETROLOGY, VOLCANOLOGY
and applied topics on *Environment*, *Archeometry* and *Cultural Heritage*

Special Issue in memory of Sergio Lucchesi

A first report on anion vacancies in a defect $MgAl_2O_4$ natural spinel

Rosa Anna Fregola[1,*], Ferdinando Bosi[2] and Henrik Skogby[3]

[1]Dipartimento Geomineralogico, Università degli Studi di Bari "Aldo Moro", Italy
[2]Dipartimento di Scienze della Terra, Sapienza Università di Roma, Italy
[3]Department of Mineralogy, Swedish Museum of Natural History, Box 50007, SE-104 05 Stockholm, Sweden
[*]Corresponding author: *r.fregola@geomin.uniba.it*

Abstract

The chemical and structural features of a natural spinel sensu stricto (s.s.) sample were studied by a multi-analytical approach, including electron microprobe analysis (EMP), Fourier transform infrared spectroscopy (FTIR), and single crystal X-ray diffraction structural refinement (SREF). The sample, coming from impure dolomitic marbles of Pegu (Myanmar), has an anomalous chemistry with an Mg-content exceeding that of the ideal formula. In addition, a chemical zoning along a line-scan of EMP analyses was observed, with Mg and Al amounts showing opposite trends. The comparatively high and low concentrations, respectively, of divalent and trivalent cations lead to a deficit of positive charges. Thus, the requirement of neutrality of global charges for crystal structures appears to be violated, in this case. The possible reasons accounting for the anomalous chemistry are discussed. Based on the combined EMP, FTIR and SREF results, it is concluded that anion vacancies can adequately compensate for the observed deficit of positive charges. Thus, the analysed sample is a defect spinel. This is the first report of anion vacancies in a natural spinel s.s. With reference to the ideal formula $MgAl_2O_4$, the formation of anion vacancies, coupled to an excess of Mg and a deficiency of Al, may be described by the substitution mechanism $2Mg^{2+}+{}^{V}\square \rightarrow 2Al^{3+}+O^{2-}$, where ${}^{V}\square$ represents an oxygen vacancy.

Key words: natural spinel; exceeding Mg-content; chemical zoning; anion vacancies.

Introduction

Spinels are widely studied materials because of the implications of their crystal structure and chemistry on topics dealing with Earth Sciences as well as Material Science.

The oxide spinel sensu lato (s.l.) structure can accommodate a very large number of cations of different valence states. It is based on a nearly cubic close-packed arrangement of oxygen atoms, with tetrahedrally (*T*) and octahedrally (*M*) coordinated sites. One-eighth of *T* and one-

half of *M* sites are filled by A and B cations, the latter mainly being divalent and trivalent cations, respectively. The distribution of cations in spinel s.l. may be written $^{IV}[A_{(1-x)}B_x]^{VI}[A_xB_{(2-x)}]O_4$, where x is the inversion parameter. Two ordered configurations are stable at low temperature, one with $x = 0$ (normal spinel), such as magnesiochromite (Lavina et al., 2003), and the other with $x = 1$ (inverse spinel), such as magnetite (Bosi et al., 2009). With increasing temperature, there will be a tendency for both normal and inverse spinels to disorder toward the random, maximum entropy, cation arrangement at $x = 2/3$. Spinels that have cation distribution with $x < 2/3$ are termed "largely normal", while those with $x > 2/3$ are known as "largely inverse" (O'Neill and Navrotsky, 1984; O'Neill et al., 2005). According to this nomenclature, spinel sensu stricto (s.s.), with ideal composition $MgAl_2O_4$, is a largely normal spinel. Non-stoichiometric spinels are also reported in the literature. Most of these studies deal with cation vacancies at the *T* and *M* sites (e.g., Lucchesi and Della Giusta, 1994; Bosi et al., 2004).

In the present paper, a natural defect spinel s.s. (labelled SP170) from Pegu (Myanmar) was studied. Structural defects of some other specimens of spinel s.s. from the same origin were earlier studied (Fregola et al., 2000; Fregola, 2001; Fregola et al., 2005), and compared to those of samples from different origin (Fregola and Scandale, 2007). The sample SP170 is a twinned crystal whose twinning features will be reported in a separate paper. In the present paper, results on its chemical and structural features will be discussed.

The interest in studying this sample stands on its peculiar chemistry, with anomalously high Mg and low Al contents, and the present work aims at clarifying the reasons for the observed excess of divalent cations and deficiency of trivalent cations.

Materials and Methods

The sample investigated (SP170) is a pink-coloured nearly pure spinel s.s. coming from impure dolomitic marbles of Pegu (Myanmar, formerly Burma) formed by contact metamorphism. It is a twinned crystal with a peculiar morphology (Figure 1), and with lateral dimensions 2.28 x 1.95 mm, as determined by an optical microscope. Its thickness, 1.076 mm, was determined by a digital micrometer after the sample was prepared. The specimen preparation was made by mechanical thinning, using SiC powders, and double-sided polishing, using diamond pastes, parallel to the largest {111} morphological faces. The spinel sample was studied by means of electron microprobe analysis (EMP), Fourier transform infrared spectroscopy (FTIR), and single crystal X-ray diffraction structural refinement (SREF). All of

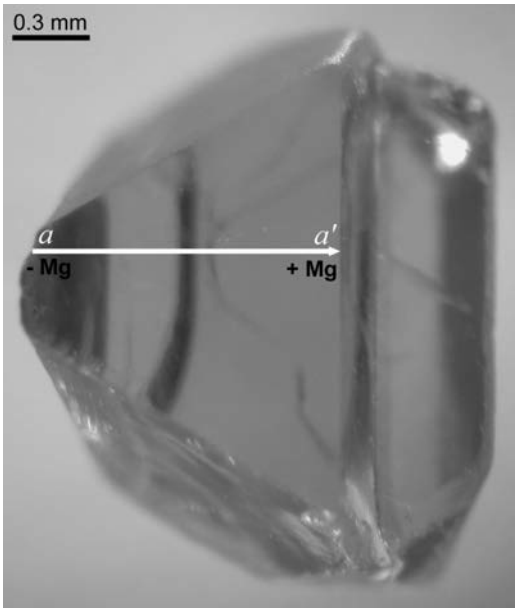

Figure 1. Optical micrograph of the natural spinel s.s. labelled SP170. *a-a'*: trace of the line-scan of EMP analyses. The Mg content increases moving from *a* to *a'*.

the analyses reported in this work were performed on one and the same twin individual (the A individual), so that they could not be affected by twinning in any case.

EMP analyses by wave dispersive spectroscopy (WDS) were carried out using a CAMECA-Camebax electron microprobe at "Istituto di Geoscienze e Georisorse", CNR Padova (Italy), under operating conditions of 15 kV (electron beam accelerating voltage) and 50 nA (beam current). The analysed elements were: Al, Mg, Fe, Zn, Cr, V, Ti, Mn, Si, and Ni. The synthetic standards used for the calibration of the spectrometers were: Al_2O_3; MgO; Fe_2O_3; ZnS; Cr_2O_3; V_2O_3; $MnTiO_3$; $Ca_3Si_3O_9$, and NiO. The counting times at the peak and at the background, respectively, were: 10 s and 5 s for the major elements; 20 s and 10 s for the minor elements. The PAP correction program of the ZAF effects, supplied by the CAMECA, was used to convert X-ray counts into oxide weight percentages.

EMP analyses were performed along the line-scan *a-a'* (Figure 1) crossing the whole extension of the (111) surface of the A individual. The length of *a-a'* was 1350 μm, with a 45 μm step length: a total of 31 analyses were carried out. As the first results showed rather high total oxide weight percentages during the acquisition of the EMP data, the line-scan was stopped at spot number 8 to verify the calibration of spectrometers. Similarly high total percentages were obtained also after the calibration, so that any unwanted effect due to instrumental problems as well as systematic errors can be excluded. Three of 31 spot analyses (#1, #2, and #8) were discarded, due to their comparatively low total percentages and because they were affected by the operation of calibrating the spectrometers. The remaining 28 analyses are reported in the "Results" section. The analytical errors (± 1σ) were estimated from background countings at sampling points.

FTIR spectra were recorded at Department of Mineralogy, Swedish Museum of Natural History (Stockholm, Sweden), in transmission mode using a Bruker Equinox 55 spectrometer equipped with a halogen lamp source, a CaF_2 beam-splitter and an InSb detector. The doubly polished spinel crystal was placed on a 300 μm circular aperture, and spectra were acquired in the 2000-12000 cm^{-1} range at a resolution of 4 cm^{-1}. The spectra were normalised to 1 mm thickness.

Two representative crystal fragments of spinel s.s. were selected from SP170 for X-ray diffraction measurements. The latter were performed with a Bruker KAPPA APEX-II single-crystal diffractometer, at Sapienza University of Rome (Earth Sciences Department), equipped with CCD area detector (6.2 × 6.2 cm^2 active detection area, 512 × 512 pixels) and a graphite crystal monochromator, using MoKα radiation from a fine-focus sealed X-ray tube. The sample-to-detector distance was 4 cm. More than 6600 exposures per sample (step = 0.2°, time/step = 10 s) covering a full reciprocal sphere were collected. The orientation of the crystal lattice was determined from 500 to 1000 strong reflections ($I > 50\ \sigma_I$) evenly distributed in the reciprocal space, and used for subsequent integration of all recorded intensities. Final unit-cell parameters were refined from 2194 to 2523 recorded reflections with $I > 10\ \sigma_I$ in the range $8° < 2\theta < 90°$. The intensity data were processed and corrected for Lorentz, polarization and background effects with APEX2 software program of Bruker AXS. Absorption correction was accomplished with an empirical method (multi-scan). No violation of $Fd\bar{3}m$ symmetry was noted. Sporadic appearance of forbidden space-group reflections, such as 046, was recognized as double reflections by their anomalously narrow reflection profiles.

Structural refinements were carried out with the SHELXL program (Sheldrick, 2008). Setting the origin at $\bar{3}m$, initial atomic positions for oxygen atoms were taken from the structure of spinel (Bosi et al., 2007). Variable parameters were overall scale factor, extinction coefficient,

atomic coordinates, site scattering values expressed as mean atomic number (m.a.n.), and atomic displacement factors. No chemical constraint was applied during the refinement. To obtain the best values of statistical indexes ($R1$ and $wR2$) the oxygen site was modeled with neutral *vs.* full ionized oxygen scattering curves, while neutral curves were used for the cation sites. In detail, the *M* and *T* sites were modeled considering the presence of Al and Mg scattering factors, respectively. Three full-matrix refinement cycles with isotropic displacement parameters for all atoms were followed by anisotropic cycles until convergence was attained. No correlation over 0.7 between parameters was observed at the end of refinement.

Results

Electron microprobe analyses

Results of 28 spot analyses performed along the line-scan *a-a'* (Figure 1) are reported in Table 1. They showed that SP170 has a rather high Mg-content as well as a low Al-content, compared to the ideal formula of spinel s.s.. The EMP data were used to calculate the atomic proportions, i.e. atoms per formula unit (apfu). At first, they were calculated on the basis of 4 anions per formula unit, as required by the spinel stoichiometry. However, such calculations showed an apparent anomaly: the sum of cations was systematically higher than 3.

As an alternative, the atomic proportions of the spinel SP170 were calculated on the basis of 3 cations per formula unit (Table 1). By fixing the sum of cations at 3, positive charges sum up to values lower than 8 and, as a consequence, the number of oxygen atoms is decreased below 4 apfu to achieve charge balance (Table 1).

A chemical zoning, i.e. a systematic variation of the chemical composition observed along the *a-a'* line-scan (Figure 2), is also noteworthy. In detail, the Mg concentration increases moving from *a* to *a'*, determining a "Mg-poorer" and a "Mg-richer" region in the crystal. Such variation is negatively correlated to that of Al (Figure 3). Obviously, also the charges as well as the oxygen proportions decrease along the line-scan, accordingly (Table 1).

Fourier transform infrared spectroscopy

The infrared spectra obtained in two different regions of the crystal ("Mg-poorer" and "Mg-richer") are nearly identical and display a strong absorption feature in the range 3000-7000 cm^{-1}. A typical spectrum normalized to 1 mm thickness is shown in Figure 4. This band structure is caused by *d-d* electronic transitions in $^{IV}Fe^{2+}$, being split by the dynamic Jahn-Teller effect, as has been earlier described (Skogby and Halenius, 2003; Lenaz et al., 2004). The observed intensity of the band indicates a $^{IV}Fe^{2+}$ site occupancy of 0.004 apfu. This value is consistent with the average one obtained by EMP analyses, that is 0.003(1) apfu.

Any absorption due to OH^- ions incorporated in the spinel structure was not observed. OH stretching bands normally occur in the 3000-3700 cm^{-1} range, and are expected to be much narrower than the Fe^{2+} bands. For comparison, the spectrum of an OH-bearing synthetic spinel (Lenaz et al., 2008) with approximately 90 ppm H_2O is shown in Figure 4. We observe no indications of narrow-band absorption in the spectra of the SP170 sample in this range, and estimate that the sample is virtually OH-free, within a detection limit of 20 ppm H_2O.

Single crystal X-ray diffraction structural refinements

X-ray diffraction measurements were performed on two crystal fragments properly selected from sample SP170. These fragments are representative of the "Mg-poorer" and "Mg-richer" crystal regions (Figure 1).

Refinement details and structural parameters, such as the unit-cell constants, oxygen fractional coordinates, bond lengths, m.a.n., and atomic

Table 1. Results of chemical analyses performed along the EMP line-scan *a-a'* on the (111) surface of the spinel s.s. SP170. The atomic proportions were calculated on the basis of 3 cations per formula unit. Analytical errors (± 1σ) in brackets. Spot: sampling point.

spot	#3	#4	#5	#6	#7	#9	#10	#11	#12	#13	#14	#15	#16	#17
MgO	28.47(10)	28.70(10)	28.78(10)	28.85(10)	28.87(10)	28.80(10)	28.77(10)	28.74(10)	28.76(10)	28.78(10)	28.92(10)	28.86(10)	28.77(10)	29.01(10)
Al_2O_3	70.35(14)	70.39(14)	70.34(14)	70.37(14)	70.37(14)	70.42(14)	70.17(14)	70.32(14)	70.25(15)	70.22(14)	69.96(14)	70.35(15)	69.59(14)	69.92(14)
SiO_2	0.01(1)	0.01(1)	0.01(1)	0.01(1)	0.02(1)	0.03(1)	0.02(1)	0.01(1)	0.02(1)	0.01(1)	0.01(1)	0.02(1)	0.01(1)	0.02(1)
TiO_2	0.24(1)	0.24(1)	0.24(1)	0.26(1)	0.24(1)	0.26(1)	0.26(1)	0.26(1)	0.25(1)	0.24(1)	0.24(1)	0.24(1)	0.23(1)	0.24(1)
V_2O_3	0.32(2)	0.34(2)	0.34(2)	0.32(2)	0.34(2)	0.33(2)	0.32(2)	0.32(2)	0.33(2)	0.34(2)	0.34(2)	0.36(2)	0.32(2)	0.33(2)
Cr_2O_3	0.58(3)	0.54(3)	0.51(3)	0.52(3)	0.53(3)	0.51(3)	0.51(3)	0.51(3)	0.49(3)	0.50(3)	0.50(3)	0.52(3)	0.48(3)	0.49(3)
MnO	0.01(1)	0.00	0.00	0.00	0.00	0.00	0.00	0.00	0.03(2)	0.00	0.02(2)	0.00	0.00	0.00
FeO	0.13(2)	0.12(2)	0.11(2)	0.11(2)	0.11(2)	0.14(2)	0.12(2)	0.14(2)	0.14(2)	0.15(2)	0.14(2)	0.18(2)	0.11(2)	0.14(2)
NiO	0.00	0.00	0.00	0.00	0.00	0.00	0.01(2)	0.02(2)	0.01(2)	0.00	0.01(2)	0.01(2)	0.00	0.01(2)
ZnO	0.41(6)	0.45(6)	0.48(6)	0.37(6)	0.47(6)	0.36(6)	0.50(6)	0.42(6)	0.40(6)	0.43(6)	0.47(6)	0.49(6)	0.44(6)	0.40(6)
Σ	*100.52*	*100.79*	*100.81*	*100.81*	*100.95*	*100.85*	*100.68*	*100.74*	*100.68*	*100.67*	*100.61*	*101.03*	*99.95*	*100.56*
						Atomic proportions on the basis of 3 cations per formula unit (apfu)								
Si	0.000	0.000	0.000	0.000	0.000	0.001	0.000	0.000	0.000	0.000	0.000	0.000	0.000	0.000
Ti	0.004	0.004	0.004	0.005	0.004	0.005	0.005	0.005	0.004	0.004	0.004	0.004	0.004	0.004
Al	1.964	1.959	1.956	1.956	1.954	1.957	1.954	1.957	1.956	1.955	1.949	1.953	1.951	1.948
Cr	0.011	0.010	0.010	0.010	0.010	0.010	0.010	0.010	0.009	0.009	0.009	0.010	0.009	0.009
Fe^{3+}	0.000	0.000	0.000	0.000	0.000	0.000	0.000	0.000	0.000	0.000	0.000	0.000	0.000	0.000
Fe^{2+}	0.003	0.002	0.002	0.002	0.002	0.003	0.002	0.003	0.003	0.003	0.003	0.004	0.002	0.003
Mn	0.000	0.000	0.000	0.000	0.000	0.000	0.000	0.000	0.001	0.000	0.000	0.000	0.000	0.000
Mg	1.005	1.010	1.013	1.014	1.014	1.013	1.014	1.012	1.013	1.014	1.019	1.013	1.020	1.022
V^{3+}	0.006	0.006	0.006	0.006	0.006	0.006	0.006	0.006	0.006	0.006	0.006	0.007	0.006	0.006
Ni	0.000	0.000	0.000	0.000	0.000	0.000	0.000	0.000	0.000	0.000	0.000	0.000	0.000	0.000
Zn	0.007	0.008	0.008	0.006	0.008	0.006	0.009	0.007	0.007	0.008	0.008	0.009	0.008	0.007
Σ	*3.000*	*3.000*	*3.000*	*3.000*	*3.000*	*3.000*	*3.000*	*3.000*	*3.000*	*3.000*	*3.000*	*3.000*	*3.000*	*3.000*
Pos. charges	7.989	7.984	7.981	7.982	7.980	7.984	7.980	7.983	7.981	7.980	7.974	7.979	7.974	7.973
Mg+Zn	1.012	1.018	1.021	1.021	1.022	1.019	1.022	1.019	1.020	1.021	1.027	1.022	1.028	1.029
Al+Cr+V+Ti	1.985	1.979	1.977	1.977	1.975	1.978	1.975	1.977	1.976	1.976	1.969	1.974	1.970	1.967
Σ O	*3.995*	*3.992*	*3.991*	*3.991*	*3.990*	*3.992*	*3.990*	*3.991*	*3.991*	*3.990*	*3.987*	*3.990*	*3.987*	*3.986*
Neg. charges	7.989	7.984	7.981	7.982	7.980	7.984	7.980	7.983	7.981	7.980	7.974	7.979	7.974	7.973

Table 1. ...continued

spot	#18	#19	#20	#21	#22	#23	#24	#25	#26	#27	#28	#29	#30	#31
MgO	28.93(10)	28.88(10)	29.06(10)	28.99(10)	29.00(10)	29.11(10)	29.13(10)	29.06(10)	29.23(10)	29.07(10)	29.28(10)	29.15(10)	29.34(10)	29.66(10)
Al_2O_3	70.02(14)	69.52(14)	69.96(14)	69.83(14)	70.04(14)	69.51(14)	69.80(14)	69.24(14)	69.61(14)	69.99(14)	69.94(14)	69.53(14)	69.23(14)	68.32(14)
SiO_2	0.01(1)	0.01(1)	0.02(1)	0.02(1)	0.01(1)	0.01(1)	0.01(1)	0.02(1)	0.02(1)	0.02(1)	0.02(1)	0.01(1)	0.02(1)	0.02(1)
TiO_2	0.23(1)	0.25(1)	0.24(1)	0.23(1)	0.24(1)	0.22(1)	0.25(1)	0.24(1)	0.24(1)	0.25(1)	0.27(1)	0.24(1)	0.24(1)	0.29(1)
V_2O_3	0.32(2)	0.33(2)	0.34(2)	0.34(2)	0.34(2)	0.35(2)	0.33(2)	0.33(2)	0.35(2)	0.33(2)	0.36(2)	0.33(2)	0.33(2)	0.34(2)
Cr_2O_3	0.50(3)	0.49(3)	0.48(3)	0.52(3)	0.57(3)	0.54(3)	0.52(3)	0.51(3)	0.48(3)	0.52(3)	0.51(3)	0.49(3)	0.57(3)	0.64(3)
MnO	0.00	0.00	0.00	0.00	0.02(2)	0.00	0.00	0.00	0.00	0.00	0.00	0.01(2)	0.02(2)	0.00
FeO	0.17(2)	0.14(2)	0.14(3)	0.14(2)	0.14(2)	0.12(2)	0.14(3)	0.14(2)	0.14(2)	0.17(2)	0.12(2)	0.13(2)	0.13(2)	0.13(2)
NiO	0.02(2)	0.01(2)	0.00	0.00	0.01(2)	0.00	0.00	0.01(2)	0.03(3)	0.01(2)	0.03(2)	0.04(3)	0.01(2)	0.00
ZnO	0.51(6)	0.38(6)	0.37(6)	0.40(6)	0.46(6)	0.43(5)	0.45(6)	0.33(6)	0.47(6)	0.41(6)	0.47(6)	0.44(5)	0.43(6)	0.36(6)
Σ	*100.71*	*100.01*	*100.61*	*100.47*	*100.83*	*100.29*	*100.63*	*99.88*	*100.57*	*100.77*	*101.00*	*100.37*	*100.32*	*99.76*
						Atomic proportions on the basis of 3 cations per formula unit (apfu)								
Si	0.000	0.000	0.000	0.000	0.000	0.000	0.000	0.000	0.000	0.000	0.000	0.000	0.000	0.000
Ti	0.004	0.004	0.004	0.004	0.004	0.004	0.004	0.004	0.004	0.004	0.005	0.004	0.004	0.005
Al	1.949	1.947	1.947	1.947	1.947	1.941	1.943	1.940	1.939	1.946	1.940	1.940	1.932	1.915
Cr	0.009	0.009	0.009	0.010	0.011	0.010	0.010	0.010	0.009	0.010	0.009	0.009	0.011	0.012
Fe^{3+}	0.000	0.000	0.000	0.000	0.000	0.000	0.000	0.000	0.000	0.000	0.000	0.000	0.000	0.000
Fe^{2+}	0.003	0.003	0.003	0.003	0.003	0.002	0.003	0.003	0.003	0.003	0.002	0.003	0.003	0.003
Mn	0.000	0.000	0.000	0.000	0.000	0.000	0.000	0.000	0.000	0.000	0.000	0.000	0.000	0.000
Mg	1.019	1.023	1.023	1.022	1.020	1.028	1.026	1.030	1.030	1.022	1.027	1.029	1.036	1.052
V^{3+}	0.006	0.006	0.006	0.006	0.006	0.007	0.006	0.006	0.007	0.006	0.007	0.006	0.006	0.006
Ni	0.000	0.000	0.000	0.000	0.000	0.000	0.000	0.000	0.001	0.000	0.001	0.001	0.000	0.000
Zn	0.009	0.007	0.006	0.007	0.008	0.008	0.008	0.006	0.008	0.007	0.008	0.008	0.008	0.006
Σ	*3.000*	*3.000*	*3.000*	*3.000*	*3.000*	*3.000*	*3.000*	*3.000*	*3.000*	*3.000*	*3.000*	*3.000*	*3.000*	*3.000*
Pos. charges	7.973	7.972	7.972	7.972	7.973	7.966	7.968	7.966	7.964	7.972	7.967	7.964	7.958	7.945
Mg+Zn	1.027	1.030	1.030	1.029	1.028	1.036	1.034	1.036	1.038	1.030	1.035	1.036	1.043	1.058
Al+Cr+V+Ti	1.969	1.967	1.967	1.967	1.969	1.962	1.963	1.961	1.958	1.966	1.961	1.960	1.953	1.939
Σ O	*3.987*	*3.986*	*3.986*	*3.986*	*3.987*	*3.983*	*3.984*	*3.983*	*3.982*	*3.986*	*3.983*	*3.982*	*3.979*	*3.973*
Neg. charges	7.973	7.972	7.972	7.972	7.973	7.966	7.968	7.966	7.964	7.972	7.967	7.964	7.958	7.945

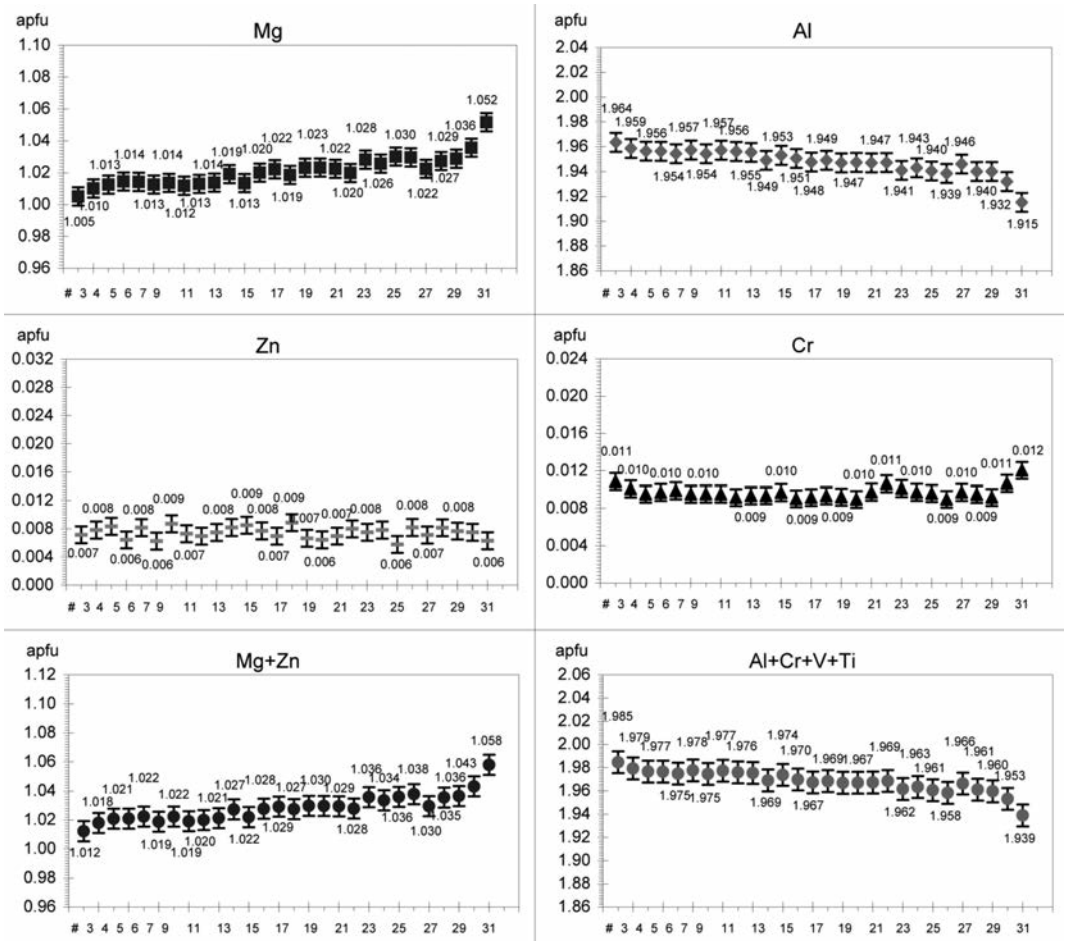

Figure 2. Graphs of EMP data showing the chemical zoning of SP170 along the *a-a'* line-scan. Mg and Al contents exhibit an opposite trend moving from *a* to *a'*. apfu: atoms per formula unit. #: number of sampling points (spots).

displacement parameters, are summarized in Table 2. In general, the values of the structural parameters increase from the "Mg-poorer" to the "Mg-richer" regions. The observed increase of the unit-cell parameter, moving from the fragment representative of the "Mg-poorer" crystal region to the "Mg-richer" one, is particularly noteworthy. This increase, in fact, reflects the replacement of small cations, such as Al, by large cations, such as Mg (Figure 3). It is also worthy to note that the calculated crystal density decreases from the "Mg-poorer" to the "Mg-richer" regions (Table 2). The weak residual electron densities observed (Table 2) are located in general positions.

Structural formulae

The intracrystalline cation distribution of the "Mg-poorer" and "Mg-richer" fragments of sample SP170 were calculated by an optimization

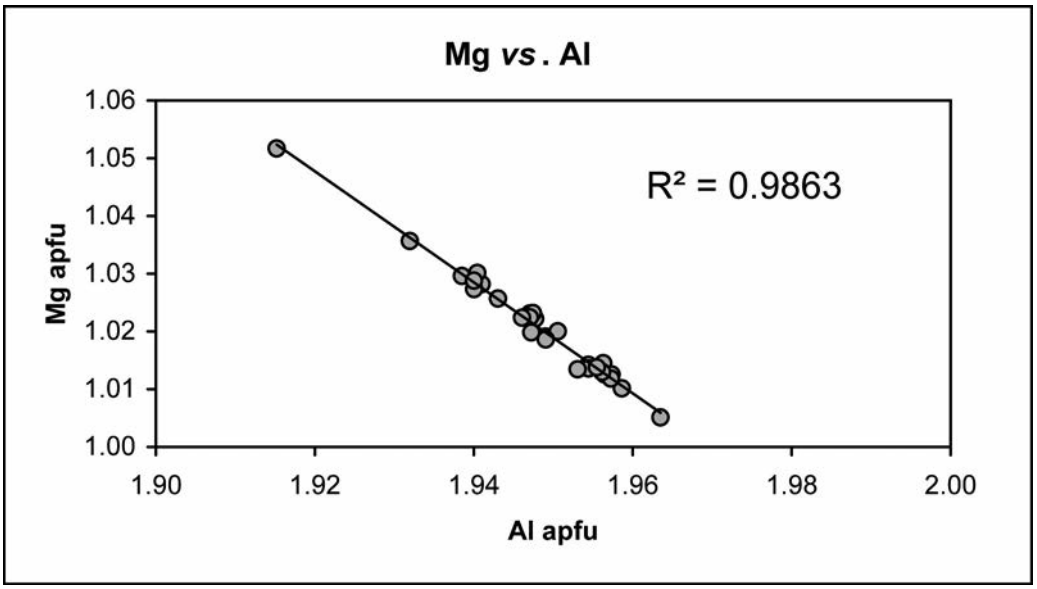

Figure 3. Graph showing the nearly perfect negative correlation of Mg vs. Al contents along the *a*-*a*' line-scan.

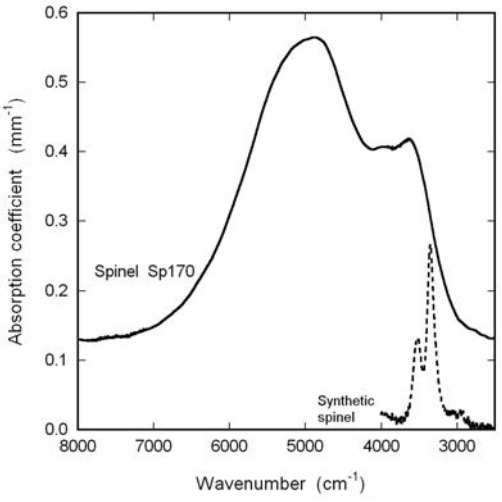

Figure 4. FTIR spectra of spinel s.s, normalized to 1 mm absorber thickness. The spectrum of the natural sample SP170 (full line) is compared to that of an OH-bearing (ca. 90 ppm H_2O) synthetic one (dashed line), the latter studied by Lenaz et al. (2008), to indicate where OH bands are to be expected.

program applying a minimization function in which both structural and chemical data are taken into account. Details on the minimization procedure are presented in Lavina et al. (2002). Final structural formulae are the following:
"Mg-poorer" fragment
$^{T}(Al_{0.15}Mg_{0.84}Zn_{0.01})\ ^{M}(Al_{1.83}Mg_{0.16}Cr_{0.01})\ O_{3.99}$;
"Mg-richer" fragment
$^{T}(Al_{0.13}Mg_{0.86}Zn_{0.01})\ ^{M}(Al_{1.81}Mg_{0.18}Cr_{0.01})\ O_{3.97}$.

Both fragments show a disordering of Mg and Al over *T* and *M* sites, with a degree of inversion $x < 0.2$. In detail, with respect to the "Mg-poorer" fragment, the "Mg-richer" one contains 0.02 apfu more of ^{T}Mg as well as ^{M}Mg, and 0.02 apfu less of ^{T}Al as well as ^{M}Al.

Discussion

The results of chemical analyses on the spinel s.s. SP170 showed two main important features: 1) a significant excess of Mg (the latter being always higher than 1 apfu), coupled with a

Table 2. Miscellaneous X-ray diffraction data of the two analyzed crystal fragments of the spinel s.s. SP170.

Crystal fragment	Sp170 "Mg-poorer"	SP170 "Mg-richer"
Space group	$Fd\bar{3}m$	$Fd\bar{3}m$
Z	8	8
Crystal size (mm)	0.13 x 0.12 ´ 0.07	0.11 x 0.10 x 0.09
Radiation, Mo-$K\alpha$ (Å)	0.71073	0.71073
Temperature (K)	293(2)	293(2)
Total number of frames	6637	6634
a (Å)	8.0872(4)	8.0900(2)
u	0.26319(3)	0.26321(2)
T-O (Å)	1.9357(4)	1.9367(3)
M-O (Å)	1.9210(2)	1.92156(17)
T-m.a.n.	12.15(5)	12.19(4)
M-m.a.n.	12.96(2)	13.00(2)
T-U^{11} (Å^2)	0.00450(10)	0.00454(8)
M-U^{11} (Å^2)	0.00397(8)	0.00401(6)
M-U^{12} (Å^2)	–0.00023(3)	–0.00025(3)
O-U^{11} (Å^2)	0.00539(9)	0.00533(7)
O-U^{12} (Å^2)	–0.00019(5)	–0.00018(4)
ρ (g/cm)	3.573	3.569
μ (mm^{-1})	1.313	1.311
F(000)	592	592
Range for data collection, θ (°)	4.36 - 45.12	4.36 - 45.10
Reciprocal space range hkl	$-16 \le h \le 13$	$-9 \le h \le 14$
	$-14 \le k \le 16$	$-16 \le k \le 14$
	$-12 \le l \le 11$	$-16 \le l \le 16$
EXTI	0.0381(18)	0.0286(9)
Set of measured reflections	2520	3553
Set of reflections with $I > 10\,\sigma(I)$	2194	2523
Unique reflections	128	133
R int. (%)	2.27	1.38
$R1$ (%) all	1.00	0.71
$wR2$ (%)	2.55	1.84
Diff. Peaks ($\pm e$/Å^3)	–0.36; 0.18	–0.20; 0.11

Notes: a = unit-cell parameter; u = oxygen fractional coordinate; T-O and M-O = tetrahedral and octahedral bond lengths, respectively; T- and M-m.a.n.. = T- and M-mean atomic number; U^{11} = atomic displacement parameter; $U^{11} = U^{22} = U^{33}$ and $U^{12} = U^{13} = U^{23}$ (= 0 for T-site due to symmetry reasons); ρ = expected crystal density; μ = linear absorption coefficient; F(000) = total number of electrons in the unit cell; EXTI = extinction parameter; R int. = merging residual value; $R1$ = discrepancy index, calculated from F-data; $wR2$ = weighted discrepancy index, calculated from F^2-data; Diff. Peaks = maximum and minimum residual electron density. Origin fixed at $\bar{3}m$.

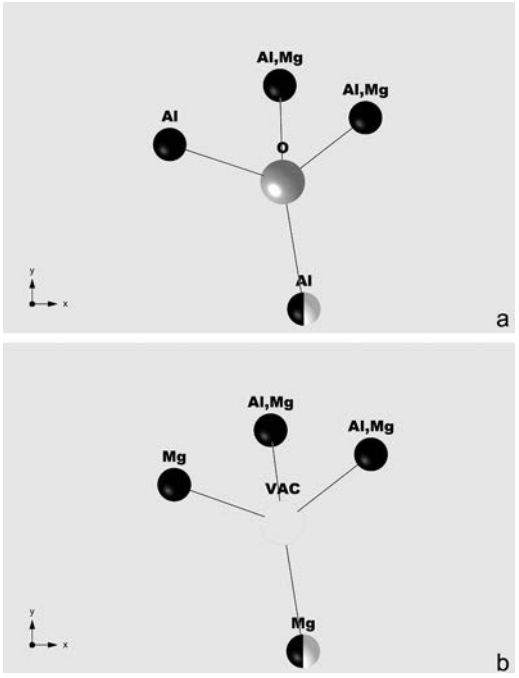

Figure 5. Local environment of the O^{2-} oxygen anion (grey circle) in the spinel structure: three cations at M (black circle) and one cation at T (two tone circle) are bonded to the O-anion. (a) Local arrangement (^{T}Al O ^{M}Al) that may occur in stoichiometric $MgAl_2O_4$ spinel. (b) Local defect arrangement (^{T}Mg $^{V}\square$ ^{M}Mg) that occurs through the substitution $^{T}Mg^{2+}+^{M}Mg^{2+} + {}^{V}\square \rightarrow {}^{T}Al^{3+}+{}^{M}Al^{3+}+O^{2-}$.

deficiency of Al (Table 1); 2) a systematic and opposite variation of Mg- and Al- contents across the crystal (Figures 2 and 3). If sample SP170 is assumed to be stoichiometric, the comparatively Mg-high and Al-low concentrations would lead to a deficit of positive charges. As a result, the charge neutrality of the crystal would be violated.

A possible explanation for this anomalous chemical composition might be that the crystal contains H^+ ions, compensating for the observed deficit of positive charges. In fact, the possibility for the spinel structure to incorporate H^+ has previously been demonstrated for non-stoichiometric synthetic samples (Fukatsu et al., 2002; Fukatsu et al., 2003; Lenaz et al., 2008). On the contrary, OH in natural spinel has not been reported so far. FTIR measurements carried out in two different regions of the crystal SP170 (i.e. "Mg-poorer" and "Mg-richer") showed no absorption bands due to OH^- (Figure 4). These observations allow the conclusion that the sample is virtually OH-free, within a detection limit of 20 ppm H_2O. Accordingly, the presence of hydrogen cannot account for the observed anomalous chemistry of sample SP170. This finding is also in line with previous studies on OH-bearing non-stoichiometric "Al-rich" and "Mg-poor" synthetic spinels s.s. (Fukatsu et al., 2002; Fukatsu et al., 2003). These authors reported that hydrogen solubility increases with increasing excess amount of alumina, and that, on the contrary, the amount of hydrogen incorporated in the spinel structure of Mg-rich compositions is extremely limited. In addition, the presence of hydrogen in the spinel structure seems to be strictly linked to the presence of cation vacancies in the tetrahedrally coordinated *T*-sites (Lenaz et al., 2008), with a probable local hydrogen position at the oxygens coordinating a vacant *T* site.

An other possible explanation for the anomalous chemistry of this sample may be that exceeding Mg cations occupy a few interstitial positions (Fleet, 1982). Also this hypothesis can be discarded, because the positions of the weak residual electron density observed (Table 2) are not correlated to those reported by Fleet (1982), thus leaving out the possibility of interstitial cations occupying a few usually empty sites of the spinel structure.

On the other hand, the anomalous chemistry of sample SP170 can be explained as due to anion vacancies in a defect spinel (Table 1). This interpretation is also supported by the increase of the unit-cell parameter, from 8.0872(4) Å to 8.0900(2) □, observed in the "Mg-poorer" and "Mg-richer" fragments, respectively. The latter

increase is strictly linked to an increase of both *T*-O and *M*-O bond-lengths (Table 2), which, in turn, is due to an increase of the Mg^{2+}-content at the *T* and *M* sites. A similar phenomenon was also observed by Serry et al. (1998) on a synthetic spinel s.s.. These authors reported that, by using a stoichiometric spinel as starting material and doping it with exceeding MgO content, a spinel with anion vacancies and increased unit-cell parameter is produced. In contrast, on doping the pure stoichiometric spinel grains with up to about 5% excess Al_2O_3, the $MgAl_2O_4$ spinel becomes cation deficient with a decreasing unit-cell parameter.

In conclusion, all of the experimental data obtained are consistent with the presence of anion vacancies, which has previously not been reported for natural spinels. In general, anion vacancies are expected to preferentially occur under conditions of low oxygen fugacities. In the present case, the anion vacancies of the spinel sample SP170, which formed in impure dolomitic marbles, might be the result of the interaction between the precursor carbonate rocks and an oxygen-poor magmatic fluid during metamorphism (Yui et al., 2008).

Mechanism of formation of anion vacancies

The information on chemical zoning (Figure 2) and the optimized structural formulae of the "Mg-richer" and "Mg-poorer" fragments of spinel SP170 indicate that the anion vacancies increase with increasing Mg^{2+}-content, whereas O^{2-}- and Al^{3+}-contents decrease. As the total number of cations remains constant, O^{2-} vacancies may be created according to the mechanism $2Mg^{2+} + {}^{V}\square \rightarrow 2Al^{3+} + O^{2-}$, where ${}^{V}\square$ represents an oxygen vacancy. With respect to stoichiometric $MgAl_2O_4$ spinel, the replacement of Al^{3+} and O^{2-} by Mg^{2+} and ${}^{V}\square$ would lead to a decrease of the crystal density, since the total mass of Al and O is larger than that of Mg. Indeed, such a decrease was observed in the crystal density (ρ) calculated from the SREF data (Table 2): ρ of the "Mg-richer" fragment (3.569 g/cm^3) is slightly lower than that of the "Mg-poorer" one (3.573 g/cm^3). Moreover, along with the formation of oxygen vacancies, the structural formulae of "Mg-richer" as well as "Mg-poorer" fragments also indicate that Al is replaced by Mg at both the *T* and *M* sites. The substitution of Mg for Al cations at the *T* and *M* sites causes an effective excess charge of -1, which is balanced by the effective charge deficiency of +2 associated with the oxygen vacancies. These substitutional and vacancy defects will invoke local charge imbalances if they are randomly distributed in the spinel structure. However, in order to reduce the local charge imbalances, the defects may preferentially order to form defect arrangements of the type ${}^{T}Mg^{V}\square^{M}Mg$, as illustrated in Figure 5.

Acknowledgements

The spinel specimen SP170 was kindly supplied by Sergio Lucchesi. Raul Carampin is acknowledged for technical support during the acquisition of EMP analyses. Comments by the reviewers, Antonio Della Giusta and Sabrina Nazzareni, were greatly appreciated. Part of this work was made for the Ph.D. thesis of RAF. Financial support from the Italian PRIN 2008 "SPIN GEO-TECH" is gratefully acknowledged.

References

Bosi F., Andreozzi G.B., Ferrini V. and Lucchesi S. (2004) - Behavior of cation vacancy in keno-tetrahedral Cr-spinels from Albanian eastern belt ophiolites. *American Mineralogist*, 89, 1367-1373.

Bosi F., Hålenius U., Andreozzi G.B., Skogby H. and Lucchesi S. (2007) - Structural refinement and crystal chemistry of Mn-doped spinel: A case for tetrahedrally coordinated Mn^{3+} in an oxygen-based structure. *American Mineralogist*, 92, 27-33.

Bosi F., Hålenius U. and Skogby H. (2009) - Crystal chemistry of the magnetite-ulvöspinel series. *American Mineralogist*, 94, 181-189.

Fleet M.E. (1982) - The structure of magnetite: defect structure II. *Acta Crystallographica*, B38, 1718-1723.

Fregola R.A. (2001) - Growth defects and growth marks of spinels from Pegu (Burma). PhD Thesis, University of Bari, 68 p.

Fregola R.A., Melone N. and Scandale E. (2005) - X-ray diffraction topographic study of twinning and growth of natural spinels. *European Journal of Mineralogy*, 17, 761-768.

Fregola R.A., Scandale E. and De Lorenzo G. (2000) - XRDT study of spinel magnesium aluminate natural crystals. ½ <121> {1$\bar{3}$5} growth dislocations. *Materials Chemistry and Physics,* 66, 149-154.

Fregola R.A. and Scandale E. (2007) - Cross-twinning in a natural spinel from Sri Lanka. *Physics and Chemistry of Minerals*, 34, 529-541.

Fukatsu N., Kurita N., Shiga H., Murai Y. and Ohashi T. (2002) - Incorporation of hydrogen into magnesium aluminate spinel. *Solid State Ionics*, 152-153, 809-817.

Fukatsu N., Kurita N., Oka Y. and Yamamoto S. (2003) - Incorporation of hydrogen into magnesium -doped α-alumina. *Solid State Ionics*, 162-163, 147-159.

Lavina B., Reznitskii L. and Bosi F. (2003) - Crystal chemistry of some Mg, Cr, V normal spinels from Sludyanka (Lake Baikal, Russia): influence of V^{3+} on structural stability. *Physics and Chemistry of Minerals*, 30, 599-605.

Lavina B., Salviulo G. and Della Giusta A. (2002) - Cation distribution and structure modelling of spinel solid solutions. *Physics and Chemistry of Minerals*, 29, 10-18.

Lenaz D., Skogby H., Princivalle F. and Hålenius U. (2004) - Structural changes and valence states in the $MgCr_2O_4$ - $FeCr_2O_4$ solid solution series. *Physics and Chemistry of Minerals*, 31, 633-642.

Lenaz D., Skogby H., Nestola F. and Princivalle F. (2008) - OH incorporation in nearly pure $MgAl_2O_4$ natural and synthetic spinels. *Geochimica and Cosmochimica Acta*, 72, 475-479.

Lucchesi S. and Della Giusta A. (1994) - Crystal chemistry of non-stoichiometric Mg-Al spinels. *Zeitschrift für Kristallographie*, 209, 714-719.

O'Neill H.S.C. and Navrotsky A. (1984) - Cation distributions and thermodynamic properties of binary spinel solid solutions. *American Mineralogist*, 69, 733-753.

O'Neill H.S.C., James M., Dollase W.A. and Redfern S.A.T. (2005) - Temperature dependence of the cation distribution in $CuAl_2O_4$ spinel. *European Journal of Mineralogy*, 17, 581-586.

Serry M.A., Hammad S.M. and Zawrah M.F.M. (1998) - Phase composition and microstructure of refractory $MgAl_2O_4$ spinel grains. *British Ceramic Transactions*, 97, 275-282.

Sheldrick G.M. (2008) - A short history of SHELX. *Acta Crystallographica*, A64, 112-122.

Skogby H. and Hålenius U. (2003) - An FTIR study of tetrahedrally coordinated ferrous iron in the spinel-hercynite solid solution. *American Mineralogist*, 88, 489-492.

Yui T.F., Zaw K. and Wu C.M. (2008) - A preliminary stable isotope study on Mogok ruby, Myanmar. *Ore Geology Reviews*, 34, 192-199.

Submitted, October 2010 - Accepted, January 2011